



LAWRENCE
LIVERMORE
NATIONAL
LABORATORY

Carbon nanotube porins in amphiphilic block-copolymers as fully-synthetic mimics of biological membranes

J. Sanborn, X. Chen, Y. Yao, J. Hammons, R. Tunuguntla, Y. Zhang, C. Newcomb, J. Soltis, J. De Yoreo, A. Van Buuren, A. Parikh, A. Noy

November 5, 2018

Advanced Materials

Disclaimer

This document was prepared as an account of work sponsored by an agency of the United States government. Neither the United States government nor Lawrence Livermore National Security, LLC, nor any of their employees makes any warranty, expressed or implied, or assumes any legal liability or responsibility for the accuracy, completeness, or usefulness of any information, apparatus, product, or process disclosed, or represents that its use would not infringe privately owned rights. Reference herein to any specific commercial product, process, or service by trade name, trademark, manufacturer, or otherwise does not necessarily constitute or imply its endorsement, recommendation, or favoring by the United States government or Lawrence Livermore National Security, LLC. The views and opinions of authors expressed herein do not necessarily state or reflect those of the United States government or Lawrence Livermore National Security, LLC, and shall not be used for advertising or product endorsement purposes.

Carbon nanotube porins in amphiphilic block-copolymers as fully-synthetic mimics of biological membranes

Jeremy R. Sanborn^{1,2}, Ramya H. Tunuguntla¹, Yuliang Zhang¹, Christina Newcomb⁴, Jennifer Soltis⁴, James J. De Yoreo^{4,5}, Atul N. Parikh², Aleksandr Noy^{1,3,*}

¹Physical and Life Sciences Directorate, Lawrence Livermore National Laboratory, Livermore, CA 94550, USA

²University of California Davis, Davis, CA 95616, USA

³School of Natural Sciences, University of California Merced, Merced, CA 95343, USA

⁴Pacific Northwest National Laboratory, Richland WA 99354, USA

⁵Departments of Materials Science and Engineering and of Chemistry, University of Washington, Seattle, WA 98195, USA

Correspondence to: noy1@llnl.gov

Abstract.

Biological membranes provide a fascinating example of a separation system that is multifunctional, tunable, precise and efficient. Biomimetic membranes, which mimic the architecture of cellular membranes, have the potential to deliver significant improvements in specificity and permeability. Here we report on a fully synthetic biomimetic membrane that incorporates ultra-efficient 1.5 nm diameter carbon nanotube porin (CNTPs) channels in a block copolymer matrix. We demonstrate that CNTPs maintain high proton and water permeability in these membranes. When embedded in discrete polymersomes, CNTPs allow small molecules to shuttle between vesicular compartments, mimicking the behavior of biological gap junctions.

Introduction.

Energy-efficient molecular separations are fundamental to a number of modern industrial, environmental, and biomedical processes including large-scale water treatment, water desalination, kidney dialysis, sterile filtration, and manufacturing of pharmaceuticals^[1]. Although synthetic polymeric membranes have come to dominate this application landscape, ever increasing demands continue to fuel the search for energy-efficient membranes that can provide both high selectivity and high permeability in the critical ca. 1 nm pore size.

To this end, biological membranes represent an attractive alternative. To achieve high levels of selectivity and permeability for separation and transport of nanometer-scale solutes, cellular membranes adopt a structural paradigm that is fundamentally different from conventional polymer membrane materials. Cellular membranes use a solute-impermeable, amphiphilic bilayer matrix that incorporates a variety of highly specific nanopore proteins (e.g., porins, gated ion-channels, connexins, etc.), which shuttle molecular or ionic solutes across the cellular or sub-cellular boundaries and enable highly selective material exchange between the cells and their surroundings^[2, 3].

Taking inspiration from biology, researchers made several efforts to pursue robust and scalable synthetic membranes that either incorporate or inherently emulate functional biological transport units. Recent studies demonstrated successful lipid bilayer incorporation of a number of artificial nanopores based on dendritic dipeptide scaffold^[4], G-quaruplexes^[5] and self-assembled pillar^[5]arenes^[6]. Other notable classes of artificial membrane nanopores include peptide-based nanopores, 3D membrane cages^[7], and large and complex DNA origami nanopores^[8]. We have recently introduced another class of artificial membrane nanopores based on carbon nanotube scaffolds: carbon nanotube porins (CNTPs)^[9]. CNTPs are short segments of lipid-coated, single-wall carbon nanotubes produced by sonication-cutting^[10] that can insert into lipid membranes and form defined ca. 1 nm diameter membrane pores with atomically-smooth hydrophobic walls that support transport of protons and water^[11, 12]. In addition, larger 1.5 nm diameter CNTPs enable transport of ions, macromolecular polymers, or ssDNA. CNTPs are unique among biomimetic nanopores because carbon nanotubes are robust and highly chemically resistant, which make them amenable for use in a wider range of separation processes including those that requiring harsh environments. Unfortunately, the lipid bilayer matrix, into which the CNTPs are embedded,

almost completely negates these advantages since it is fragile and disassembles in non-aqueous environments or upon exposure to air.

A robust and flexible membrane matrix is thus another critical component of an artificial membrane. Many amphiphilic block co-polymers form bilayer motifs (i.e., polymersomes) in their dilute suspensions^[13, 14], making them a leading alternative to lipid-based liposomal membranes. Compared to liposomes, polymersomes are mechanically more robust, and offer a wider range of membrane elasticities and degrees of passive membrane permeability^[13]. For instance, higher bending moduli of polymer vesicles, 40-460 $k_B T$ (compared to 10-30 $k_B T$ for lipid vesicles) make them less prone to bending deformations and their lower stretching moduli (80-100 mN/m vs. 250-1000 mN/m for vesicles) render them more resistant to strain induced fractures, allowing them to withstand volume expansion/compression under osmotic stresses^[15]. Moreover, compared to lipid membranes, polymer membranes have lower water permeabilities (0.7 -10 $\mu\text{m}/\text{s}$ vs. 15-150 $\mu\text{m}/\text{s}$) and reduced lateral fluidities (0.1-0.01 $\mu\text{m}^2/\text{s}$ vs. 1-4 $\mu\text{m}^2/\text{s}$). Furthermore, a thicker hydrophobic core in polymer membranes (8-10 nm vs. 3-4 nm for lipid bilayers) should provide a better match for the 10-12 nm long CNTPs.

Here we report integration of CNTP channels into poly(butadiene)-polyethylene oxide (PBD₂₂-PEO₁₄) polymer membranes, mimicking the structure, architecture, and basic functionality of biological membranes in an all-synthetic architecture. Proton and water transport measurements show that carbon nanotube pores maintain their high permeability in the polymer membrane environment. In a significant expansion of the CNTP platform capabilities, we also demonstrate that CNTPs embedded in polymersomes can transport small molecule reagents between vesicular compartments opening new opportunities for delivery molecular reagents to vesicular

compartments to initiate confined chemical reactions and mimic the sophisticated transport-mediated behaviors of biological gap junctions.

Methods.

Materials. We used 1.5 nm diameter P2 CNTs (Carbon Solutions Inc.) to produce CNTPs. P2 CNTs contain a higher concentration of defects than the raw CNT stock that we used in previous studies^[10, 11] (as indicated by an increased D-band signal in the Raman spectra, see Suppl. Mater. Fig 1) and we found that these defects resulted in more efficient cutting and an increased yield of CNTPs. 1,2-dioleoyl-sn-glycero-3-phosphocholine (DOPC) and Rhodamine B 1,2-dioleoyl-sn-glycero-3-phosphoethanolamine (DOPE) were obtained from Avanti Polar Lipids. PBD-PEO 1800 polymer (P10191) was obtained from Polymer Source Inc. Horseradish peroxidase (P6782), 8-Hydroxypyrene-1,3,6-trisulfonic acid trisodium salt (HPTS, H1529), luminol sodium salt (A4685), calcium chloride, hydrogen peroxide (216763), phosphate buffered saline (P4417), 4-(2-Hydroxyethyl)piperazine-1-ethanesulfonic acid (HEPES, RDD002), hydrochloric acid solution (H9892), sodium chloride (S7653), potassium chloride (P9333), and deuterium oxide (151882) were obtained from Sigma Aldrich. Fluo-4 pentapotassium salt (F14200) was obtained from Thermo Fisher Scientific Inc. Preassembled extruders with 200nm and 400nm pore sizes were obtained from T&T Scientific Inc.

Vesicle preparation. PBD-PEO di-block copolymer vesicle were made following previously described protocols with minor changes^[16]. Briefly, 5 mg of PBD-PEO 1800 suspended in chloroform was deposited in a glass vial and dried under vacuum overnight to remove all traces of chloroform. The film was resuspended in buffer and heated to 70 °C for 30 minutes before stirring at 200 RPM for an additional 30 minutes to form multilamellar vesicles. To convert them into unilamellar vesicles the solution was subjected to 10 freeze-thaw cycles and then heated to 70 °C prior to mechanical extrusion through 400 nm or 200 nm tract-etched membranes. To incorporate 1.5 nm diameter CNTPs into the polymersomes, we adapted the protocols developed for incorporating CNTPs into lipid vesicles^[17]. We first dehydrated 0.5-1.5 ml of the appropriate CNTP solution for 30 minutes in a rotating desiccator heated to 50 °C. Dried film was hydrated with buffer (see next section for details) and briefly bath-sonicated to ensure complete solubilization. This DOPC/CNT complex was then used to hydrate a dried PBD-PEO film to obtain a final polymer concentration of 5 mg ml⁻¹. The solution was then heated to 70 °C and stirred for 1 h, then it underwent 10 cycles of the freeze-thaw treatment, followed by extrusion through a 400 nm polycarbonate filter. Finally, polymersomes were

separated from unincorporated CNTPs with size-exclusion chromatography on an 8 cm long Sepharose CL-6B column. Purified vesicles were characterized with dynamic light scattering (DLS) (Zetasizer Nano-ZS90, Malvern Instruments) with each measurement containing an average of at least 10 individual runs. DOPC and DOPC-CNTP liposomes were made as described previously^[17].

Measurements of proton permeability. Polymersomes and CNT-Polymersome proton transport measurements followed the protocols previously described for measuring proton transport in DOPC-CNTP liposomes^[11]. Briefly, polymersome-CNTP vesicles containing 10 mM of the pH-sensitive HPTS dye in buffer (150 mM NaCl, 30 mM KCl, and 10mM HEPES, pH of 7.5). Separately, 2 ml of the same buffer adjusted to pH 6.9 was placed in a cuvette inside a fluorimeter (Fluoromax 4, Horiba) and equilibrated to room temperature for at least 5 min with constant stirring. 70 μ L vesicle aliquots were added to the cuvette and the instrument recorded a time trace of the HPTS fluorescence (Em/Ex: 450 nm/514 nm). Proton permeability was determined from these kinetics as described previously^[11].

Direct estimation of diblock copolymer/phospholipid concentration by a colorimetric assay. The amount of membrane amphiphile present in samples was measured using a colorimetric assay that was used previously for lipids^[18] and diblock copolymers^[19]. Briefly, 200 μ L aliquots of samples were dried for 15 minutes in a rotating desiccator heated to 50C. The dried samples were then solubilized with 2 ml of chloroform, followed by the addition of 2 ml ammonium ferrothiocyanate. This solution was vortexed vigorously for 1 min and allowed to separate on the bench top. The bottom chloroform layer was carefully extracted with a Pasteur pipette and the absorbance was measured at 510 nm (488 nm) to quantify the polymer (lipid) mass. This analysis used a calibration curve prepared from samples of known lipid and polymer concentrations.

High-speed AFM (HS-AFM) imaging of supported block-copolymer bilayers. All AFM imaging used a substrate consisting of a 1.5 mm diameter mica disk glued on a glass rod of the HS-AFM sample stage. Mica surfaces were freshly cleaved prior to sample deposition and a small aliquot of vesicles was placed on the sample with a pipette and incubated for 30 minutes at 70C. HS-AFM images of CNTPs were acquired in tapping mode at room temperature using an HS-AFM instrument (RIBM, Japan) equipped with ultra-short AFM cantilevers with custom-produced high-density carbon/diamond-like carbon (HDC/DLC) tips (USC-F1.2-k0.15, NanoWorld, tip radius < 10 nm). The electron beam deposited (EBD) carbon tips (radius < 10 nm) were also fabricated on the AFM cantilevers with the Zeiss Crossbeam 1540. For all imaging studies the HS-AFM fluid cell was filled with 120 μ L of phosphate buffered saline. 128 x 128 pixel images were collected from a 200 x 200 nm area at a scan rate of 2 frames per second.

The home-built Matlab2015 (MathWorks, Natick, MA) code was used to convert the raw HS-AFM images to ImageJ (National Institutes of Health, Bethesda, MD) stacks for further processing.

Cryogenic TEM measurements of CNTP-Polymersomes. Specimens were prepared for cryogenic (cryo) TEM specimens by placing a 3- μ L drop of sample onto a 200 mesh copper TEM grid coated with lacey carbon film (EMS). Grids were glow discharged prior to use (EasiGlow, Ted Pella). Grids were inserted into an FEI Vitrobot Mark IV (FEI, Hillsboro, OR) maintained at room temperature and 70 % relative humidity and blotted with filter paper (blot time: 1 s, relaxation time: 1 s, blotting force: 1 (unitless parameter)). The grid was then rapidly plunged into liquid ethane. All specimens were stored and handled under liquid nitrogen after vitrification. Specimens were imaged under low-dose conditions in a FEI Titan 80-300 Environmental TEM equipped with a field emission electron gun and operated at 300 kV. Specimens were transferred into the TEM while maintaining cryogenic conditions (-176 °C) by using a Gatan 626 cryo-TEM holder. Images were captured with an UltraScan 1000 2k x 2k charge capture device (CCD) camera (Gatan, Inc.) operated via Digital Micrograph (Gatan, Inc). Once recorded, images that were processed using ImageJ.

NIR absorption measurements. NIR absorption was measured using a Cary 4000 UV-Vis/NIR spectrometer (Agilent). Briefly, 100 μ L of vesicles were aliquoted into glass vials and dehydrated in a rotary evaporator set to 55 °C until completely dry. Dried film was then resuspended with 200 μ L of D₂O water and bath-sonicated until the sample solution appeared uniformly turbid. The absorbance was measured from 1800 nm to 200 nm at a scanning rate of 600 nm/s and a time interval of 0.1 s. The absorbance in the S₂₂ regime (900-1100 nm)^[20] was selected and subtracted from measurements of polymer or lipid vesicles alone to determine the peak absorbance.

Water transport studies. Water permeabilities of CNTP-polymersomes or control polymersomes were determined using a stopped-flow instrument (SFM2000, BioLogic) and previously described protocols^[12]. Briefly, vesicles were rapidly mixed in the stopped-flow instrument with a hypertonic buffer solution composed of 10 mM HEPES (pH 7.5) and varying concentrations of HPTS (from 6.25 to 40 mM) or poly(diallyldimethylammonium chloride (PDADMAC) (0.5% to 4% (w/v)). The osmolarity of each buffer was verified with a freezing-point osmometer (Osmomat 3000, Gonotec) prior to the experiment. Light scattering data was acquired in the time interval between 50-500 μ s, at 90° scattering angle, and a measured dead time of 0.7 msec. For each osmolyte concentration, we averaged at least 3

individual runs and the resulting kinetics were used to calculate the water permeability as described previously^[12]. The reported value for water permeability was calculated from an average of 3 different vesicle preparations.

Raman Spectroscopy of CNTPs. Raman spectra of dried CNTP aliquots were collected using a Nicolet Almega XR micro-Raman spectrometer at laser wavelengths of 633 nm and laser power was kept below 100 W/cm to avoid heating the samples.

Chemiluminescence assay. CNTP-polymersomes containing 50 U/mL of horseradish peroxidase were formed in a 10mM HEPES buffer at pH 7.8. To prevent damage to the enzyme we used 4 freeze-thaw cycles in the vesicle preparation instead of the 10 listed above. Once extruded and separated from un-encapsulated protein with size exclusion chromatography, vesicle fractions were collected, combined, and used immediately. In a typical experiment, 100 μ L of CNTP-polymersomes loaded with horseradish peroxidase were added to a cuvette containing 1.8 mL of 10 mM HEPES, pH 7.8. After 5 minutes, 40 μ L of 200 mM luminol sodium salt and 66.7 μ L of 30% hydrogen peroxide was added, in separate steps, to begin the reaction and luminol chemiluminescence signal at 432nm was recorded in a Fluoromax-4 fluorometer with the excitation pathway blocked and under constant stirring.

Ca²⁺ vesicle docking assay. CNTP-polymersomes were formed in a 10mM HEPES buffer, pH 7.2, that also contained 100 μ M of calcium indicator dye Fluo-4 pentapotassium salt. DOPC liposomes that incorporated 1 mM CaCl₂ were formed. After extrusion and size-exclusion chromatography purification both types vesicles were kept in a water bath at 23.6 °C. In a typical experiment, 100 μ L of polymersome and liposome vesicles were pipetted into 2.8 mL of 10 mM HEPES pH 7.2 in a cuvette in a fluorimeter (Fluoreomax-4, Horiba), and Fluo-4 fluorescence kinetics (Ex:494/Em:514) was recorded under constant stirring. Calculation of the concentration of calcium present inside the vesicles was determined through comparison of the normalized fluorescence intensity increase obtained from a calibration curve. Calcium concentration was determined from Fluo-4 fluorescence using a calibration curve obtained from the spectra of 270nM of Fluo-4 mixed with a series of calcium buffers (See Suppl. Mater. Fig. 2). Determination of free calcium dependence on temperature, ionic strength, pH, and EGTA concentration was calculated using literature data^[21].

Vesicle fusion assay. CNTP-polymersomes, CNTP-liposomes, pure polymersomes, and pure liposomes were formed in 10 mM HEPES buffer, pH 7.2. Pure polymersomes and liposomes contained 5% (w/w) rhodamine B DOPE such that rhodamine B fluorescence is self-quenched. In a typical experiment 100 μ L of pure liposomes and 100 μ L of CNTP-liposomes were added to a cuvette with 1.8mL 10 mM HEPES buffer (pH 7.2). Kinetics of membrane

exchange was evaluated by observing dequenching of rhodamine B fluorescence (Ex./Em. : 543/565 nm) under constant stirring.

Results and Discussion.

CNTP incorporation and characterization. We chose PBD₂₂-PEO₁₄ (PBD-PEO 1800) diblock co-polymer (MW PBD:PEO of 1200:600) as a membrane matrix since it forms 10-12 nm thick polymer bilayers that provide an ideal match for CNTP length. Block copolymer membranes were previously used to incorporate a variety of membrane proteins, such as aquaporin Z^[22], ATP synthase^[23], GPCRs^[24], and OmpF porins^[25]; therefore, we expected that CNTPs would also incorporate into this membrane. To insert CNTPs into the block-copolymer membranes, we modified previously developed procedures for inserting CNTPs into lipid matrices^[10, 17], by adding elevated temperatures and constant stirring necessary for PBD-PEO 1800 to form vesicles.

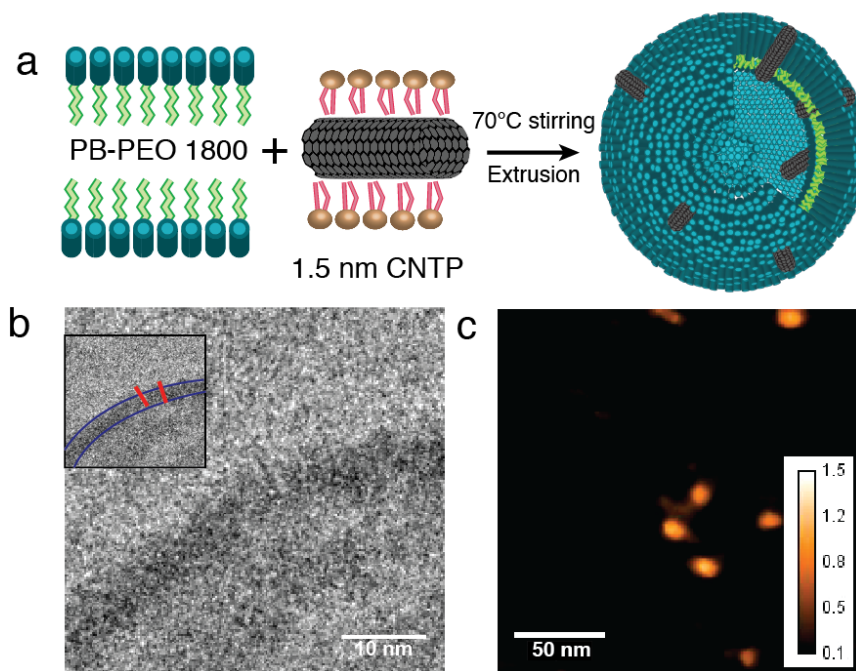


Figure 1. CNTPs in polymersome membranes. **a.** Schematic of the CNTP incorporation into PB-PEO 1800 polymersomes. **b.** Cryogenic TEM image of a polymersome wall with CNTPs. Inset highlights the location of the CNTPs in the image. **c.** A frame from a HS-AFM movie of the CNTP/polymersome membrane fused onto a mica surface. Image shows several CNTPs protruding above the polymersome membrane plane.

Cryogenic TEM (cryoTEM) images of CNTP-polymersomes (Figure 1b) revealed the presence of needle-shaped features within the polymersome membrane that likely correspond to CNTPs inserted in the membrane. These images also share broad similarity with the cryoTEM images that we reported previously for CNTPs inserted into lipid bilayers^[9], although the overall contrast between the nanotube and polymer matrix was weaker (See Suppl. Mater. Fig. 3). The majority of CNTPs in polymersome layers were oriented perpendicular to the membrane plane, although we cannot completely exclude the possibility that we missed some CNTPs inserted into the membrane at higher tilt angles due to low contrast of the cryoTEM images.

To characterize the morphology and dynamics of CNTPs in the polymersome membrane further, we fused the CNTP-containing polymersomes to a mica surface and imaged the resulting supported bilayer with high-speed atomic force microscopy (HS-AFM). We previously showed that HS-AFM not only can visualize CNTPs in lipid bilayers, but also can capture real-time dynamics of CNTP diffusion in the bilayer plane^[26]. HS-AFM movies of control polymersome layers showed flat layer morphology devoid of any sharp features. These movies and other AFM images indicated that polymersome bilayers had smooth morphology and were approximately 9 nm thick, which agrees with the ca. 7-11 nm thicknesses observed in the cryo-TEM images. In contrast, HS-AFM images of CNTP-containing polymersomes (see Supplementary Movie 1) reveal multiple sharp features protruding by on average 1-2 nm above the membrane plane, which we attribute to the CNTPs.

To quantify the CNTP content in CNTP-polymersome samples, we measured the near IR (NIR) absorbance in the 1050 nm region, which corresponds to the S_{22} transitions in carbon nanotubes. This spectral region is convenient because water and block-copolymers that we used have minimal signal in this range (See Suppl. Mater. Fig. 4), simplifying background subtraction.

CNTP-polymersome samples showed a clear adsorption peak in this region, which was absent in control samples; moreover, the magnitude of the S_{22} peak increased with the increased loading of CNTPs into the polymersomes, confirming that this signal originated from the CNTPs. To quantify the number of CNTPs in the polymer membrane we compared the magnitude of the S_{22} signal with the similar measurement performed on previously calibrated vesicle samples that contained CNTPs inserted into pure lipid bilayers. We then used this ratio of NIR signals (corrected for the difference in surface area of liposomes and polymersomes) to calculate the number of CNTPs present in polymersomes. Surprisingly, this comparison revealed that polymersome samples had 4 times more CNTPs compared to lipid samples formed under the same conditions. We attribute this effect to a better match between CNTPs length and the polymersome bilayer thickness. Furthermore, we speculate that higher elasticity of polymer bilayers may also favor the CNTP insertion. We also note that polymersome layers were previously shown to support nearly close-packed arrangement of artificial membrane channels^[6], suggesting that future work could potentially increase the CNTP loading.

Proton conductance. Proton conductance measurements provide another way to characterize the number of CNTPs present in the polymersome membranes. When CNTPs-polymersomes were loaded with pH-sensitive HPTS dye in their lumen and exposed to a small pH gradient (Figure 2a), we observed rapid pH equilibration (Figure 2b) confirming that CNTPs in the polymer membrane serve as efficient proton transport conduits. Control polymersomes without CNTPs exhibited much slower pH equilibration kinetics; this is similar to our previous measurements of proton transport in CNTPs in lipid bilayers^[11] and indicates that the bulk of the proton flux in this system indeed flows through the CNTPs. Thus, it was not surprising that increased CNTP loading, quantified by an increase in S_{22} adsorption (Figure 2c), produced a corresponding increase in the

proton flux through the CNTP polymersomes (Figure 2d). The unitary CNTP proton conductance $0.73 \cdot 10^{-7} \pm 0.41 \cdot 10^{-7}$ nS determined from these measurements (as the slope of the linear fit through the data on the Figure 2b) is within a factor of 3 of the unitary proton conductance value of $1.80 \cdot 10^{-7} \pm 0.69 \cdot 10^{-7}$ nS of CNTPs in lipid bilayers^[1] This result could be expected, as the proton conductance rate primarily reflects the arrangement of the water hydrogen bonding pattern in the nanotube, but also can reflect the different nature of the surrounding membrane matrix.

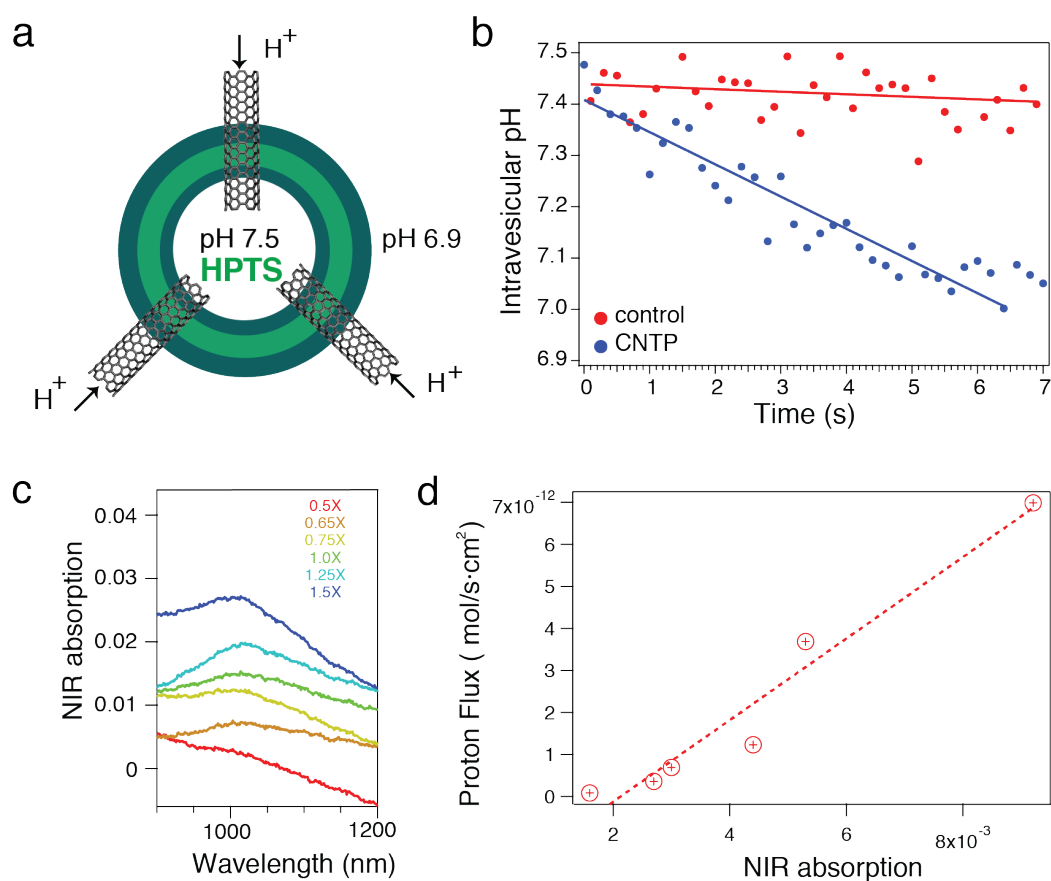


Figure 2. Proton transport through CNTPs in polymersome membranes and optical properties of CNTPs. **a.** Schematic of the experiment. **b.** Initial time traces of the lumen pH values of polymersomes after pH of the outside solution decreased from 7.5 to 7.0. **c.** NIR absorption spectra in the S₂₂ regime for increasing CNTP loading in CNTP-polymersomes. **d.** A plot of proton flux in CNTP-polymersomes as a function of NIR absorption. Dashed line indicates a linear fit through the data.

Water transport through CNTP in polymersomes. Our previous stopped-flow measurements of water transport through CNTPs embedded in lipid membranes showed that they

were highly efficient water conductors^[12]. Here we used similar protocols to investigate water transport through CNTPs in polymersomes (Figure 3). Like lipid vesicles, polymersome membranes are susceptible to complex osmotically induced shape changes, as has been previously reported for diblock polymersomes^[27]. Thus, subtraction of the background water permeability of the polymersomes is not trivial in this case. Indeed, stopped-flow kinetics recorded after we subjected PBD-PEO 1800 polymersomes to an osmotic gradient (Figure 3B) revealed that instead of following a single-exponential kinetics characteristic of gradual volume change, light scattering traces showed two distinct single-exponential kinetics regions, separated by a ‘shoulder’ region (Figure 3b). Similar stopped-flow kinetic traces have also been previously recorded for DODAB vesicles^[28]. As the osmotic stress increases, the location of the inflection point of the shoulder region shifts to earlier times (See Suppl. Mater. Fig. 5) Following the models described in the literature, we assumed that osmotic response of polymersomes involved initial shrinkage followed by a structural transition to a deformed shape – most likely a variant of the ‘stomatocyte’ shape – which then shrinks further as water transport across the membrane equalized the osmotic imbalance (Figure 3a). Thus, we chose to use the first exponential region of the kinetic trace to extract the background polymersome water permeability. Our measured vesicle water permeability of ca. 30 $\mu\text{m}/\text{s}$ is within the range of water permeability values reported for diblock copolymers, 2.5 $\mu\text{m}/\text{s}$ ^[29] - 189.7 $\mu\text{m}/\text{s}$ ^[30], even though a direct comparison with other studies may be complicated because the water permeability may be influenced by differences in aqueous buffer conditions and polymer chemistry.

Remarkably, when the polymersomes containing CNTPs were subjected to different levels of osmotic stresses, they showed much faster shrinkage kinetics and no clear shoulder was observed in the stopped-flow curves (Figure 3b,c) with only the lowest osmotic stress traces showing hints of

the ‘stomatocyte’ transition behavior. These results suggest that in the presence of a large number of CNTPs, which enable much faster water escape from the vesicle lumen, the ‘stomatocyte’ shape transition is kinetically suppressed. We speculate that the transport behavior of CNTP-laden polymersomes is governed by a topological transformation, characterized by division of polymersome compartments consistent with continuous shrinkage that we observe.

Factors driving shape deformations of liposomes and polymersomes subject to hypertonic stresses are largely understood in terms of minimal bending energy configurations of vesicles under conditions of reduced volume, $v = \frac{V}{[4\pi R_0^3/3]} < 1$ where R_0 corresponds to the radius of an equivalent sphere of area $S = [4\pi R_0^2]$ ^[31]. These treatments implicitly assume that the vesicles adopt equilibrium shapes, which correspond to the smallest possible value of the membrane bending energy^[32] and produce shape diagrams depicting shape morphologies (e.g., oblate, prolate, dumbbell, and stomatocytes) as a function of reduced volume^[33]. Experimentally however, significant deviations from the predictions from these equilibrium shape diagrams, including budding, division, and tubulations, have also been observed most frequently associated with the generation of spontaneous membrane curvature through non-homogeneous distribution of membrane molecules^[34]. Our present observations are consistent with (but do not independently establish) the idea that the high concentration of CNTPs in polymer membranes may be accompanied by generation of spontaneous curvature and lateral phase separation, which promote budding and division over stomatocyte shape transformations under hypertonic conditions.

The unitary permeability of CNTPs, measured in the stopped-flow data experiments was $7.7 \cdot 10^{-14} \pm 2.5 \cdot 10^{-14} \text{ cm}^3 \cdot \text{s}^{-1}$ (See Suppl. Mater. Fig. 6) These results agree with the water permeability that we previously reported for 1.5 nm diameter CNTPs embedded in lipid

vesicles^[12] ($5.9 \cdot 10^{-14} \text{ cm}^3 \cdot \text{s}^{-1}$), suggesting that the water transport mechanism in CNTPs is largely conserved between the two membrane scaffolds. Notably, unlike the behavior that we observed in the experiments with lipid vesicles^[12], the water permeability was independent of the osmotic stress (See Suppl. Mater. Fig. 6), which we attribute to the greater flexibility of the polymer membrane.

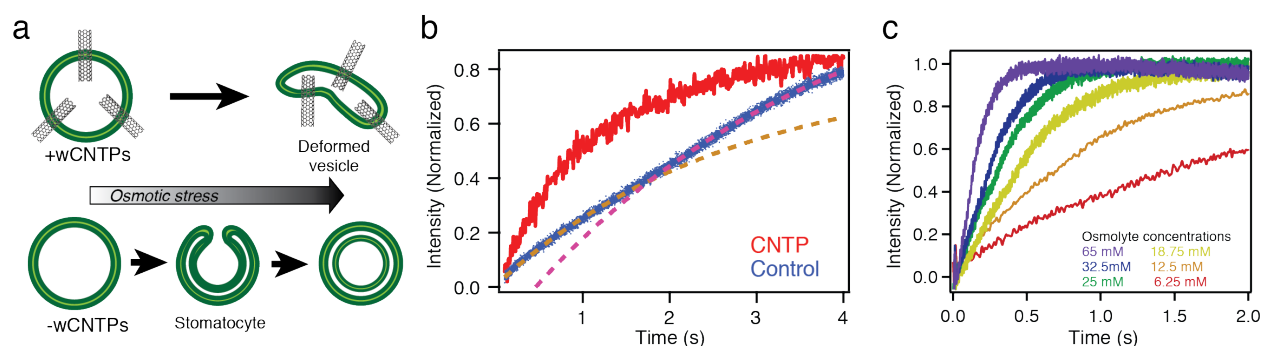


Figure 3. Water transport through CNTPs in polymersome membranes. **a.** Schematics showing different polymersome response to osmotic stress depending on the presence of CNTPs. **b.** Comparison of water transport kinetics from light scattering traces of hyperosmotic shocks of 0.5% PDADMAC acting on polymer vesicles with CNTPs and control vesicles without CNTPs, with 2 different fits (dashed lines) that approximate the general shape in the control trace. **c.** Light scattering traces taken from CNTP-polymersomes mixed with a series of HPTS concentrations.

CNTPs polymersomes as nanoreactor compartments. The experiments described in the previous sections show that CNTP channels in the walls of polymersomes facilitate mass exchange between the bulk solution and polymersome lumen. The small diameter of these channels should allow the CNTP-polymersomes to selectively encapsulate large molecules. This arrangement opens up a possibility to use CNTP polymersomes as nanoscale reactor compartments that contain and isolate some of the reaction components whereas the other components can be delivered through the CNTPs. We first used this concept to demonstrate localized chemiluminescence production in CNTP-polymersomes. We placed an enzyme, horseradish peroxidase (HRP), into the lumen of polymersomes that contained CNTPs in their walls. At 44 KDa, HRP is too large to pass through the CNTPs and thus remained trapped inside the lumen. However the 1.5 nm CNTPs were still

large enough to transport small organic molecules^[35] such as luminol and hydrogen peroxide that react with HRP to produce chemiluminescence. Indeed, when we added luminol to this sample, we observed a strong increase in the chemiluminescence (Figure 4a). In contrast, when the polymersomes lacked the CNTP channels in the wall, addition of luminol did not increase chemiluminescence, showing that the encapsulated enzyme and the substrate remained spatially separated. These experiments demonstrated that 1.5 nm CNTPs facilitate the transport of small molecules and highlight the potential of CNTP-based nanoreactors to conduct cell-free reactions in the conditions that can simulate crowded intracellular environments.

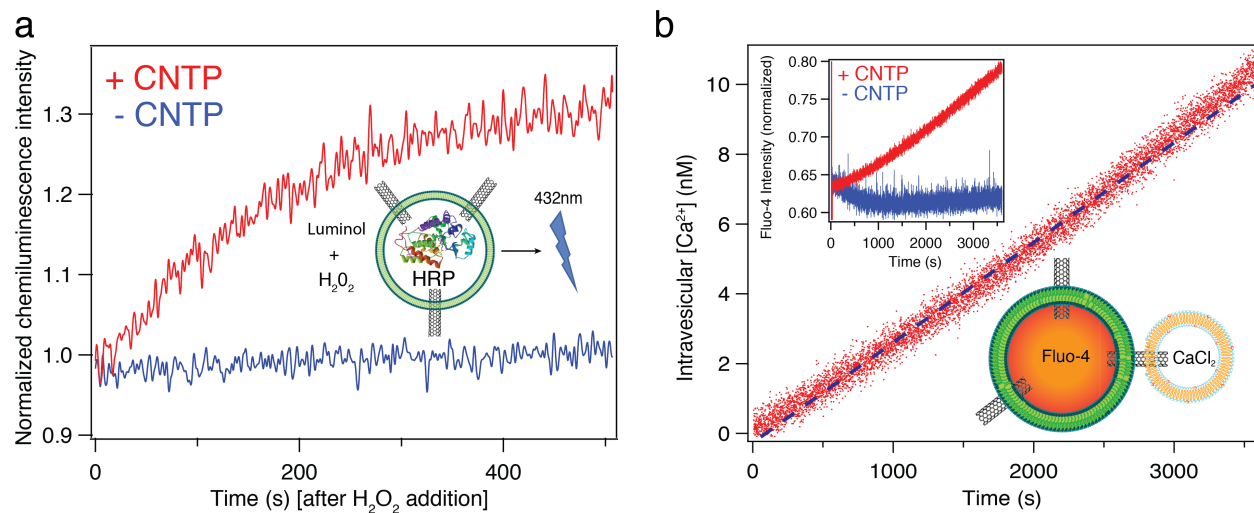


Figure 4. CNTPs as connectors for nanoscale compartments. **a.** Chemiluminescence intensity recorded after adding luminol and hydrogen peroxide to the solution of polymersomes sequestering horseradish peroxidase (HRP) enzyme in presence (red trace), and in absence (blue trace) to CNTPs in the polymersomes. **b.** A graph showing an increase in Ca^{2+} ion levels inside polymersomes caused by diffusion of Ca^{2+} ions from liposomes to polymersomes through CNTP conduits (inset schematics). The inset shows the fluorescence signal intensity traces for the Ca^{2+} reporter dye Fluo-4 encapsulated inside polymersomes, recorded in presence (red trace) and in absence (blue trace) of CNTPs in the polymersome wall.

Another interesting possibility is to use CNTPs as a nanoscale conduit for small molecule exchange between two nanoscale compartments, mimicking the functionality of connexin channels, which form gap junctions that mediate direct cell-cell exchange of small molecules^[3]. Our previous studies^[9] indicated that CNTPs have a propensity to bridge two adjacent bilayers, forming a

simplified mimic of a gap junction. Unfortunately, subsequent MD simulations also raised the possibility that this configuration could also facilitate membrane fusion after the nanotube bridges two lipid bilayers^[36]. Thus, for a CNTP to act as a gap junction mimic this undesirable process needs to be suppressed.

We hypothesized that if nanotube bridges two dissimilar membranes, e.g. a polymer and a lipid membrane, fusion cannot occur. To test this hypothesis, we labeled a fraction of lipids with a self-quenching concentration of Rhodamine B di-oleyl phosphatidylcholine (Rhodamine B-DOPE, see Methods, Suppl. Figure 6). Both the hemi-fusion and full fusion events^[37] would lead to the dilution of the labeled lipid and de-quenching of the dye. Indeed, we observed significant de-quenching (Suppl. Fig. 7, top trace) when both populations of interacting vesicles (donor vesicles that contained CNTPs, and recipient vesicles that did not) were formed with lipid bilayers. In contrast, when we used CNTP-polymerosomes as the donor vesicles, their interactions with the recipient liposomes did not show any de-quenching (Suppl. Fig. 7, bottom trace) indicating that, as expected, CNTPs did not facilitate fusion between vesicles made of dissimilar types of bilayers.

To demonstrate CNTP-mediated material exchange between two separate vesicular compartments, we encapsulated a large Ca^{2+} indicator dye Fluo-4, which should not escape through 1.5 nm diameter CNTPs, in the polymerosomes and added them to the lipid vesicles that contained 60mM CaCl_2 . As expected, we observed a steady increase in the Fluo-4 emission after mixing these two vesicle populations (Figure 4b, red trace), indicating that Ca^{2+} ions were able to diffuse into the polymerosome interior through the CNTP connections formed between the two types of vesicles. Significantly, we did not observe any evidence of Fluo-4 fluorescence increase when CNTPs were absent from the polymerosomes, (Figure 4b, blue trace), which confirmed that CNTPs were indeed responsible for Ca^{2+} diffusion between the two vesicular compartments. These experiments also

point to an interesting possibility for designing versatile CNTP gap junction mimics that would be able to tune the transport selectivity simply by using nanotube porins of different diameter.

Conclusion.

Our results show that carbon nanotube porins can insert into the block copolymer layers to form completely synthetic mimics of biological membranes. CNTPs form transmembrane pores in polymersomes similar to those formed in lipid bilayers, and we show that these pores also have similar transport properties, establishing CNTPs as a universal membrane channel mimic. In particular, CNTPs maintain high proton and water permeability similar to those we reported previously for lipid membranes. The ability to use CNTPs in non-lipid membrane matrices allowed us to construct more sophisticated transport systems with CNTPs not only facilitating transmembrane transport, but also enabling gap-junction-like communication between different population of vesicles. We believe that these findings enable a number of interesting possibilities for designing new biomaterials systems. CNTPs of different size and length can be used to control transport selectivity, to regulate the communication between compartments of synthetic proto-cells or between proto-cell and live cells, and to facilitate sophisticated cargo exchange in these systems.

Acknowledgments. JS acknowledges support by LGS program at LLNL. Polymersome incorporation and transport studies were supported by the Division of Materials Research of the National Science Foundation under an award 1710211. High-speed AFM and cryogenic TEM characterization studies were supported by the U.S. Department of Energy, Office of Basic Energy Sciences, Division of Materials Sciences and Engineering under award SCW0972. Work at the Lawrence Livermore National Laboratory was performed under the auspices of the U.S. Department of Energy under Contract DE-AC52-07NA27344. Work at the Molecular Foundry was supported by the Office of Science, Office of Basic Energy Sciences, of the U.S. Department of Energy under Contract No. DE-AC02-05CH11231.

References.

- [1] M. Mulder, *Basic Principles of Membrane Technology*, Springer, 1996; M. Shannon, P. Bohn, M. Elimelech, J. Georgiadis, B. Marinias, A. Mayes, *Nature* 2008, 452, 301; J. R. Werber, C. O. Osuji, M. Elimelech, *Nature Rev. Mater.* 2016, 16018.
- [2] Y.-x. Shen, P. O. Saboe, I. T. Sines, M. Erbakan, M. Kumar, *J. Membr. Sci.* 2014, 454, 359.
- [3] B. Alberts, D. Bray, J. Lewis, M. Raff, K. Roberts, J. D. Watson, *Molecular Biology of the Cell*, Garland Science, New York 2007.
- [4] V. Percec, A. E. Dulcey, V. S. K. Balagurusamy, Y. Miura, J. Smidrkal, M. Peterca, S. Nummelin, U. Edlund, S. D. Hudson, P. A. Heiney, H. Duan, S. N. Magonov, S. A. Vinogradov, *Nature* 2004, 430, 764.
- [5] M. Barboiu, A. Gilles, *Acc. Chem. Res.* 2013, 46, 2814.
- [6] Y.-x. Shen, W. Si, M. Erbakan, K. Decker, R. De Zorzi, P. O. Saboe, Y. J. Kang, S. Majd, P. J. Butler, T. Walz, A. Aksimentiev, J.-l. Hou, M. Kumar, *Proc. Natl. Acad. Sci. USA* 2015, 112, 9810.
- [7] B. P. Benke, P. Aich, Y. Kim, K. L. Kim, M. R. Rohman, S. Hong, I.-C. Hwang, E. H. Lee, J. H. Roh, K. Kim, *J. Am. Chem. Soc.* 2017, 139, 7432.
- [8] M. Langecker, V. Arnaut, T. G. Martin, J. List, S. Renner, M. Mayer, H. Dietz, F. C. Simmel, *Science* 2012, 338, 932; A. Seifert, K. Göpfrich, J. R. Burns, N. Fertig, U. F. Keyser, S. Howorka, *ACS Nano* 2015, 9, 1117; S. Howorka, *Nature Nanotechnol.* 2017, 12, 619.
- [9] J. Geng, K. Kim, J. Zhang, R. Tunuguntla, L. Comolli, F. Allen, K. Cho, D. Munoz, Y. Wang, C. P. Grigoropoulos, C. M. Ajo-Franklin, A. Noy, *Nature* 2014, 514, 612.
- [10] R. H. Tunuguntla, X. Chen, A. Belliveau, F. I. Allen, A. Noy, *J. Phys. Chem.* 2017, 121, 3117.
- [11] R. Tunuguntla, F. Allen, K. Kim, A. Belliveau, A. Noy, *Nature Nanotech.* 2016, 11, 639.
- [12] R. Tunuguntla, R. Henley, Y.-C. Yao, T. A. Pham, M. Wanunu, A. Noy, *Science* 2017, 357, 792.
- [13] D. E. Discher, A. Eisenberg, *Science* 2002, 297, 967.
- [14] F. M. Menger, K. D. Gabrielson, *Angew. Chem. Int. Ed.* 1995, 34, 2091; K. T. Nam, S. A. Shelby, P. H. Choi, A. B. Marciel, R. Chen, L. Tan, T. K. Chu, R. A. Mesch, B. C. Lee, M. D. Connolly, C. Kisielowski, R. N. Zuckermann, *Nature Mater.* 2010, 9, 454; S. I. Stupp, V. LeBonheur, K. Walker, L. S. Li, K. E. Huggins, M. Keser, A. Amstutz, *Science* 1997, 276, 384; L. F. Zhang, A. Eisenberg, *Science* 1995, 268, 1728.
- [15] R. R. Tangorra, A. Operamolla, F. Milano, O. H. Omar, J. Henrard, R. Comparelli, F. Italiano, A. Agostiano, V. De Leo, R. Marotta, A. Falqui, G. M. Farinola, M. Trotta, *Photochem. & Photobiol. Sci.* 2015, 14, 1844; R. J. R. W. Peters, M. Nijemeisland, J. C. M. van Hest, *Angew. Chem. Int. Ed.* 2015, 54, 9614; D. A. Christian, A. W. Tian, W. G. Ellenbroek, I. Levental, K. Rajagopal, P. A. Janmey, A. J. Liu, T. Baumgart, D. E. Discher, *Nature Mater.* 2009, 8, 843.
- [16] D. L. Gettel, J. Sanborn, M. A. Patel, H.-P. de Hoog, B. Liedberg, M. Nallani, A. N. Parikh, *J. Am. Chem. Soc.* 2014, 136, 10186.
- [17] A. E. R. H. Tunuguntla, V. Frolov, A. Noy, *Nature Protocols* 2016, 11, 2029.
- [18] J. C. M. Stewart, *Analyt. Biochem.* 1980, 104, 10.

- [19] O. Al-Hanbali, N. M. Onwuzo, K. J. Rutt, C. M. Dadswell, S. M. Moghimi, A. C. Hunter, *Analyt. Biochem.* 2007, 361, 287.
- [20] A. L. Antaris, J.-W. T. Seo, A. A. Green, M. C. Hersam, *ACS Nano* 2010, 4, 4725.
- [21] D. M. Bers, C. W. Patton, R. Nuccitelli, in *Methods in Cell Biology*, Vol. 99 (Ed: M. Whitaker), Academic Press, 2010, 1.
- [22] M. Kumar, M. Grzelakowski, J. Zilles, M. Clark, W. Meier, *Proc. Natl. Acad. Sci. USA* 2007, 104, 20719.
- [23] H.-J. Choi, C. D. Montemagno, *Nano Lett.* 2005, 5, 2538.
- [24] S. May, M. Andreasson-Ochsner, Z. Fu, Y. X. Low, D. Tan, H.-P. M. de Hoog, S. Ritz, M. Nallani, E.-K. Sinner, *Angew. Chem. Int. Ed.* 2013, 52, 749.
- [25] W. Meier, C. Nardin, M. Winterhalter, *Angew. Chem.* 2000, 112, 4747.
- [26] Y. Zhang, R. H. Tunuguntla, P.-O. Choi, A. Noy, *Phil. Trans. Roy. Soc. B* 2017, 372, 20160226.
- [27] R. Salva, J.-F. Le Meins, O. Sandre, A. Brûlet, M. Schmutz, P. Guenoun, S. Lecommandoux, *ACS Nano* 2013, 7, 9298.
- [28] D. H. W. Hubert, M. Jung, P. M. Frederik, P. H. H. Bomans, J. Meuldijk, A. L. German, *Langmuir* 2000, 16, 8973.
- [29] B. M. Discher, Y.-Y. Won, D. S. Ege, J. C.-M. Lee, F. S. Bates, D. E. Discher, D. A. Hammer, *Science* 1999, 284, 1143.
- [30] M. Kumar, J. E. O. Habel, Y.-x. Shen, W. P. Meier, T. Walz, *J. Am. Chem. Soc.* 2012, 134, 18631.
- [31] L. Miao, U. Seifert, M. Wortis, H. G. Dobereiner, *Physical Review E* 1994, 49, 5389; B. L. S. Mui, H. G. Dobereiner, T. D. Madden, P. R. Cullis, *Biophys. J.* 1995, 69, 930.
- [32] P. B. Canham, *J. Theor. Biol.* 1970, 26, 61.
- [33] S. Svetina, B. Zeks, *Eur. Biophys. J. Biophys. Lett.* 1989, 17, 101.
- [34] H. G. Dobereiner, J. Kas, D. Noppl, I. Sprenger, E. Sackmann, *Biophys. J.* 1993, 65, 1396; M. Yanagisawa, M. Imai, T. Taniguchi, *Phys. Rev. Lett.* 2008, 100, 4.
- [35] K. Kim, J. Geng, R. Tunuguntla, L. R. Comolli, C. P. Grigoropoulos, C. M. Ajo-Franklin, A. Noy, *Nano Lett.* 2014, 14, 7051.
- [36] R. M. Bhaskara, S. M. Linker, M. Vögele, J. r. Köfinger, G. Hummer, *ACS Nano* 2017, 11, 1273.
- [37] P. Wadhvani, J. Reichert, J. Bürck, A. S. Ulrich, *Eur. Biophys. J.* 2012, 41, 177.